Modelling of a free-flow photovoltaic-thermal (PV-T) water collector

Sophia Motteu and Tomas Satura

Chemical Engineering Department, Imperial College London, U.K.

Abstract—Hybrid photovoltaic-thermal (PV-T) technology, combining electrical and thermal conversion of solar energy, has drawn interest due to the enhanced overall efficiency achieved by PV-T systems. The free-flow PV-T water collector configuration presents several aspects of interest including the combined role of water as both heat transfer fluid and spectrum filter, and potential for reduced cost. In this paper, a model describing the performance of this design was developed in OpenFOAM and validated against experimental data. Multi-phase flow, heat transfer by radiation, convection and conduction, the angle of incident radiation, as well as condensation and evaporation were accounted for. The model was found to predict collector performance to an accuracy of 0.4 % and 1 % for the electrical and thermal efficiencies respectively.

Keywords—solar energy, hybrid PV-T, cooling, spectral splitting, efficiency

INTRODUCTION

With an annual potential superior to 100 TW, solar energy is the most abundant source of energy on Earth (Goswami, 2015). The increase in global energy demand associated with population and economic growth, as well as the environmental threat posed by the use of non-renewable energy sources, constitute a drive for harvesting solar energy (OECD, 2011). Despite its inexhaustible potential, the exploitation of solar energy is limited by the energy efficiency and the cost associated with solar technology. There has, therefore, been a great incentive to improve the technical potential of solar energy and increase its contribution to the world's energy demand.

Photovoltaic (PV) panels have long been used for the conversion of solar radiation into electricity, while solar thermal (ST) collectors have provided a way to extract thermal output from solar energy. An important issue in the operation of PV panels lies in the fact that solar cell materials respond only to a portion of the solar spectrum; typically, between 6 and 20 % of the radiation intercepted by the PV surface is converted to electricity (Dubey et al., 2013). Incident photons with an energy greater than the band gap of the cell material are therefore absorbed as heat, resulting in an increased temperature of the PV module. As studies have shown, the efficiency of a PV panel is significantly affected by its operating temperature, with high cell temperatures thus compromising their performance (Skoplaki and Palyvos, 2009). Besides this limitation, the use of both PV and ST technologies is constrained by the roof space available for their installation.

Since its invention in the 1970s, the hybrid photovoltaic-thermal (PV-T) technology has drawn considerable interest as it addresses the issues related to the individual PV and ST technologies by combining the two concepts (Riffat and Cuce, 2011). PV-T collectors use a heat transfer fluid to extract the waste heat from the PV panel and convert it to a useful thermal output for various applications including domestic hot water and space heating, while obtaining a higher electrical output from the cooled PV panel. Through this combination, PV-T systems offer a greater overall energy output than separate PV and ST systems covering the same total area (Matuska, 2014). These systems are therefore of particular interest in domestic applications, where installation space is limited, and their demand is expected to increase (Herrando et al., 2014).

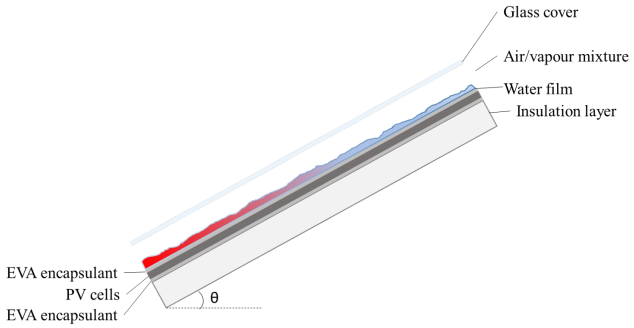

Fig. 1: Schematic illustration of a free-flow PV-T collector

Several studies have been conducted to investigate the potential of various PV-T designs (Avezov et al., 2011), (Abdelrazik et al., 2018). Particularly, innovative PV-T designs using fluid-based filters have been mentioned as promising alternative set-ups (Wang et al., 2019). This paper focuses on the free-flow PVT water collector shown in Figure 1; the system comprises of an inclined PV module covered by a glass cover, with a water film allowed to freely flow on the surface of the PV panel. In this work, a model accounting for the air-water multiphase flow in the cavity, heat transfer by radiation, convection and conduction, the angle of incident radiation, as well as condensation and evaporation of the water film, was developed and validated against experimental data.

Theory & Background

PV-T systems allow for a more productive use of the collector area by simultaneously generating electrical and thermal outputs. The requirement for low PV operating temperatures is illustrated in Figure 2 which shows the decline of solar cell performance with increasing PV surface temperature as dictated by the Evans-Florschuetz equation (Equation (9)) (Evans and Florschuetz, 1977)(Alshakhs, 2013). The thermal output of the system is directly proportional to the temperature of the heat transfer fluid circulated. The fluid outlet temperature determines the suitability of a collector for specific applications such as domestic hot water where the target draw-off temperature set by British Standards is 60°C (BSI, 2015). Although the PV-T technology enhances the overall energy output of a given collector area, a trade-off between electrical and thermal efficiencies arises from the inherent compromise between thermal output and PV operation temperature (Lämmle et al., 2017).

The performance of PV-T systems is greatly determined by design parameters including glazing, the choice of thermal fluid used, and the location of the fluid in the system. The configuration considered in this study presents several aspects of interest in terms of the choice and combination of design parameters proposed.

Studies have evaluated the effect of a glass cover on the overall performance of a PV-T system. Kim and Kim (2012) compared the thermal and electrical efficiencies of glazed (covered) and unglazed PV-T collectors. Results showed that while the unglazed PV-T offers a higher electrical efficiency due to reduced losses of solar radiation through reflection and absorption, glazing strongly enhances the system's thermal efficiency by reducing convective heat losses. Glazing was found to increase thermal efficiency by 14 % and reduce electrical efficiency by 1.4 % (Dubey et al., 2013). The beneficial impact of the glass cover on thermal losses exceeds its negative contribution to the electrical efficiency, demonstrating that glazed PV-T systems achieve a net improvement of overall efficiency.

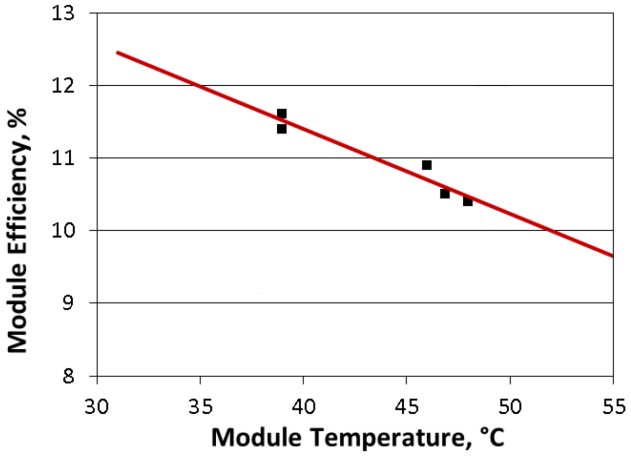

Fig. 2: Variation of solar cell efficiency as a function of operating temperature (Alshakhs, 2013)

In this configuration (Figure 1), the heat transfer fluid freely flows on the front side of the PV panel, thus placing it in direct contact with the surface to be cooled, while also allowing for the exploitation of the spectral splitting effect of the water film. Odeh and Behnia (2009) discussed the effect of using a water layer on the front surface of the PV module; they suggested that along with cooling by natural convection, refraction in the water film causes an increase in incident radiation, leading to an enhanced electrical output. Additionally, water has the potential to act as a selective-absorption filter (Vivar and Everett, 2014).

Figure 3 shows that water absorbs a large portion of the incoming solar radiation which does not correspond to the spectral response in the silicon cell. By preventing part of the solar spectrum range which is not useful to electrical conversion from reaching the PV cells, the water film can effectively reduce the temperature increase that would otherwise be observed on the PV panel surface.

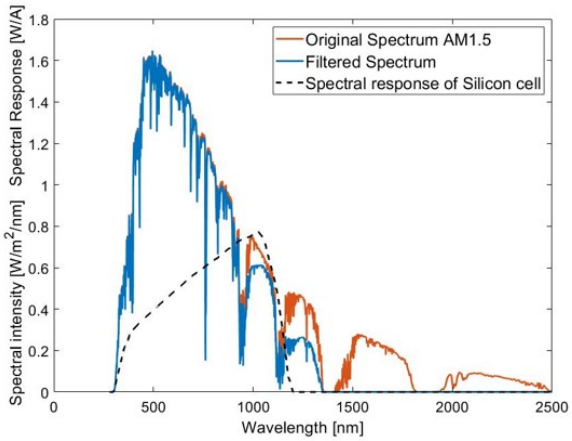

Fig. 3: Solar radiation spectrum, filtered spectrum and Si cell spectral response for a 5 mm water film (Huang, 2019)

Compared to sheet and tube or channel PV-T designs, the free-flow PV-T collector could have reduced material costs, as it eliminates the need for conduits to circulate the heat transfer fluid and requires one less glass layer than the channel case (Jiwanapurkar and Joshi, 2015). This characteristic could give the free-flow PV-T system an advantage of reduced initial investment cost compared to other configurations.

Earlier studies which considered a free-flow collector mentioned the potential effect of evaporation and condensation on the overall performance of the system. Evaporation of the water film constitutes a source of heat loss, which can affect thermal efficiency (Zondag et al., 2003), and water condensation on the glass cover can influence propagation of radiation inside the system by inducing further reflection of incoming solar radiation (Charalambous et al., 2007). The numerical model developed by Zondag et al. (2003) for the free-flow panel design does not take into account the additional reflection resulting from the phase change taking place in the cavity, and therefore does not allow to quantify the consequence of this phenomenon. The methodology developed in this paper aims to incorporate the physical phenomena important to the prediction of the free-flow collector performance, such that it can subsequently be used to maximise the potential of this specific design and optimise its output.

METHODS

The simulations were conducted in the OpenFOAM v1906 environment. There were three main physical phenomena that were treated in the simulations. Firstly, it was desirable that the simulations account for the non-uniformity of the two-phase flow arising as an effect of the free-flowing film both in terms of hydrodynamic and optical properties. Furthermore, condensation and evaporation of the medium were to be modelled. Finally, unlike in previous work where the effects of irradiance were only modelled by inserting an artificial heat source in solid and liquid phases, it was aimed that both the magnitude and angle of irradiance be simulated directly. The methodology for modelling these three phenomena is described in the subsequent subsections.

Multi-phase Nature

The simulated system encompasses solid (covering glass and the PV panel), liquid (water as heat-transfer medium) and gas (air and water vapour) components. There are generally two ways of modelling such a multi-component system – either splitting it into several regions in which corresponding solid and fluid components would be treated separately, or treating them all together as one multi-phase system. The latter was chosen for its easier implementation.

As the flow is characterized by presence of a large distinct interface between liquid and gas continuous phases, the volume-of-fluid (VOF) approach was applied. In this approach, there are four main transport equations that are solved for. The first is a general continuity of mass expressed as:

$$\frac{\partial \rho}{\partial t} + \nabla \cdot (\rho \mathbf{U}) = 0 \tag{1}$$

Secondly, the temperature field is obtained by solution of the energy transport equation. An artificial term S_h is added as a radiative contribution to the enthalpy of the system:

$$\frac{\partial \rho h}{\partial t} + \nabla \cdot (\rho \mathbf{U} h) = \nabla^2 \kappa T + S_h \tag{2}$$

Distinctively to the VOF approach, there is only a single momentum equation solved throughout the whole system, which has an additional term accounting for interfacial tension between fluid phases. Since the system was treated as multi-phase containing solid phases, an extra term is conjointly added to account for the fluid-solid interactions. Thus, the momentum equations is of form:

$$\frac{\partial \rho \mathbf{U}}{\partial t} + \nabla \cdot (\rho \mathbf{U}\mathbf{U}) = -\nabla p + \rho \mathbf{g} + \nabla (\mu \nabla \cdot \mathbf{U}) + \mathbf{F_s} + \mathbf{F_{sol}} \tag{3}$$

A phase fraction α_i is used to denote the fraction of a computational cell occupied by a phase i. There is a separate transfer equation for α_i:

$$\frac{\partial \alpha_i}{\partial t} + \nabla \cdot (\alpha_i \mathbf{U}) + \nabla \cdot (\mathbf{U}_e \alpha_i (1 - \alpha_i)) = 0 \tag{4}$$

The term $\nabla \cdot (\mathbf{U}_e \alpha_i (1 - \alpha_i))$ is specific to OpenFOAM solvers and was implemented based on work of Jasak and Weller (1998), where it was proposed to

serve a function of interface sharpening. The artificial quantity $\mathbf{U}_e$ is referred to as interfacial velocity and is defined as:

$$\mathbf{U}_e = |\mathbf{U}| \frac{\nabla \alpha_i}{|\nabla \alpha_i|} \tag{5}$$

The interaction between solid and fluid phases was accounted for using Voller-Prakash model, which adds additional energy to the interface, effectively providing a no-slip boundary condition at the interface. Theoretical background of the model was proposed in the work of Voller and Prakash (1987). This model gives rise to the term added to the momentum equation.

Solution of this system of equations yields fields describing the system. This is obtained using the `icoReactingMultiphaseInterFoam` solver of OpenFOAM (present as of the version v1806). However, further closure models are required to account for the underlying physical phenomena.

Phase Change

The evaporation and condensation is modelled using a model proposed by Carey (1992). This model is implemented in OpenFOAM environment as `kineticGasEvaporation`. It is based on Hertz-Knudsen equation:

$$\phi_{LV} = C \sqrt{\frac{M}{2\pi R T_{act}}} \left(p_{par} - p_{act}\right) \tag{6}$$

By this equation, the mass flux of liquid to vapour phase ϕ_{LV} is linked to partial pressure p_{par} and to activation temperature T_{act} and pressure p_{act}. The activation quantities physically correspond to saturation ones, however they might be chosen to have slightly different values from the corresponding saturation point, as the particular case might be better fitted by a model with differing values. The link between the pressure and temperature is provided by Clausius-Clapeyron equation as:

$$\frac{dp}{dt} = \frac{L}{T_\Delta v} \tag{7}$$

Thus, the accuracy of this model depends on the choice of the values of activation temperature and pressure, and of the evaporation frequency C. These values are empirical and are obtained from the literature.

Radiation

Incident radiative rays upon a surface are subject to transmission, absorption or reflection. The fraction of radiation absorbed by the surface increases its internal energy and thus results in increase in temperature. Therefore, radiation is accounted for in the energy equation of a computational cell by the term S_h as shown in Equation 2. This term is calculated as:

$$S_h = aG - 4\left(e\sigma_{SB}T^4 + E\right) \tag{8}$$

Hence, the term S_h has two contributions - irradiance G and emissive radiation. In this case, however, only the former is of interest, as the panel is operated at temperatures at which emissive radiation is negligible. With absorptivity of the given material a specified, this enables to evaluate S_h from G received by the computational cell. Further propagation of G is governed by specified transmissivity, which is a fraction of radiation transmitted by the material. The remainder of the radiation is assumed to be reflected. It is further possible to specify scattering model, which governs propagation of the transmitted irradiance.

With these models, it is possible to construct a field of G inside of the solved domain. However, for an application of simulation of a real PV-T panel, it is necessary to set proper boundary values of G. This corresponds to the amount of solar radiation received by the boundary, and thus depends on the position of the sun relative to the panel.

Sun Tracking

The irradiance on the boundaries is effectively given by global horizontal irradiance, which has two contributions. The first is contribution of diffuse irradiance, that arises by scattering of light in the atmosphere. The second is the direct normal irradiance, which effectively accounts for the radiation that directly penetrates the atmosphere. Nevertheless, this needs to be adjusted by the angle of the incident rays relative to the panel. Keeping the diffuse irradiance constant, the normal irradiance and its corresponding angle need to be evaluated in order to assign a proper boundary value for G.

There are in principle two pathways to obtain the value of the normal irradiance. Either it can be specified as constant with `sunLoadConstant` model, or it can be calculated using `fairWeatherConditionsModel` model. In the latter case, the value is obtained using the ASHRAE handbook (ASH, 2017).

The knowledge of the trajectory of the Earth around the Sun, the angle acuted by the Earth's axis and the line connecting the Earth's and Sun's centres of gravity, and the speeds of both Earth's rotations and revolutions is the prerequisite for computing the angle of incident radiation. The angle itself is then a function of the geographical location, time of the day and day of the year. The mathematical algorithm for computing this angle is implemented in the `sunDirTracking` model.

Simulation Setup

Tutorial cases from the directory of `icoReactingMultiphaseInterFoam` were used as base cases of the simulation. The mesh of the base case can be generated either using `blockMesh`, or

from a supplied CAD file. It is, however, important that an extra entry is added in the boundary file of the `polyMesh` directory, whereby all boundaries are added to a group `viewFactorWall`. The grouping is important for later generation of view factors.

The dictionaries needed in the constant directory are `g`, `turbulenceProperties`, `phaseProperties`, `thermoPhysicalProperties.*`, `viewFactorsDict`, `radiationProperties` and `boundaryRadiationProperties`. The dictionary `g` for the gravitational acceleration was set such that the direction of this vector points to the bottom of the used mesh. Laminar model was used for turbulence treatment, thus applying Stokes' approach. It should be noted, that in further work a suitable low Reyenolds number model can be used instead, which would, however, require its configuration with `icoReacingMultiphaseInterFoam` solver, which currently only operates with either laminar or the standard $k-\varepsilon$ model.

In the `phaseProperties`, liquid, gas and and solid phases were defined. The types of the phases used were `pureStaticSolidPhaseModel` for solids, `pureMovingPhaseModel` for liquid and `multiComponentMovingPhase` for gas. Subsequently, sub-models for phase interactions were defined. These were `sigma`, `interPhasePorous` and `massTransfer`. In the `sigma` sub-directory, the value of interfacial tension of gas-liquid phase-pair was set to 0.07 N/m and 0 N/m for all other phase-pairs, as the solid phases are to be treated as stationary. Similarly, it was important to define `massTransfer` model as `VollerPrakash` model with a very high constant (of the order of 10^{15} or higher), a workaround aimed at stopping diffusion of the fluid into the computational cells occupied by solid phases. Finally, the `massTransfer` model was set to `kineticGasEvaporation`, with numerical values for activation temperature and frequency set to 366 and 0.1 respectively, in line with the base tutorial case.

`thermoPhysicalProperties.*` set of dictionaries was created, in which token $*$ denotes each phase as declared in the `phaseProperties`. In the dictionary for gas phase, components enumerated in the entry for species were air and vapour. In the directories of the liquid and solid phases, only the component of the single phase was entered. Subsequently, the thermodynamic properties were entered in line with individual material properties.

Radiation was initialized via `radiationProperties`. Its structure was adapted from tutorial of `chtMultiRegionFoam`. Constant models were implemented for absorption, emission, scattering and transmission, with their parameters being dependant on materials of the specific simulation case. Furthermore, simulations conducted in versions v1906 and later enable treatment of reflected rays, which was also set in this dictionary.

The dictionaries `boundaryRadiationProperties` and `viewFactorsDict` were used to further support radiation modelling. In the former, specific values of emissivity, absorptivity and transmissivity were entered for each boundary in line with their physical characteristics. Besides default entries, the `viewFactorsDict` needed a specification of number of coarse faces on each patch, used in creation of agglomerated grid for solution of radiation. This is of high importance, as during generation of view factors, a member function `shortRays` is used, which has a hard coded maximum for faces it can process on all patches combined, in order to limit computational demand. Hence, the overall number of coarse faces needed to be kept to 1,200.

Selection of solvers and discretization was done in line with the `icoReactigMultiphaseInterFoam` tutorials, selecting second-order accurate discretization schemes. No correction for non-orthogonality was implemented, as it was supposed the grid would be of simple geometry composing hexahedral blocks, thus having low non-orthogonality.

Ultimately, before each simulation, it was necessary to execute `faceAgglomerate` and `viewFactorGen`, so as to set fields of view factors on the mesh.

MODEL VALIDATION

As the ultimate expected outcome of a PV-T collector simulation is establishing both electrical and thermal efficiencies, it is necessary to validate that the established code is able to simulate temperature distributions on the plate and in the water film, as well as the level water evaporation and condensation. Values of the aforementioned quantities obtained from simulations were therefore compared against experimental data.

Since experimental investigation of a PV-T panel with the design characteristics proposed in this paper was not available in the literature, the study conducted by Aybar et al. (2005) on an inclined solar water distillation system is used. Although intended for a different application, the setup considered in that work resembles in several aspects of its design and operation the free flow PV-T panel of interest. As shown in Figure 4, the set up consists of an inclined absorber plate over which a continuous water film flows; evaporation takes place in the cavity and the condensation process occurs on the glass cover. Material properties and experimental conditions for the study of the solar water distillation system were specified as detailed in Appendix Tables 1 to 3. Temperatures of the water film and plate were measu-

red experimentally and reported at intervals of one hour over the day. Additionally, the volume of water evaporated and condensed was recorded. The results of these experiments were used to carry out model validation.

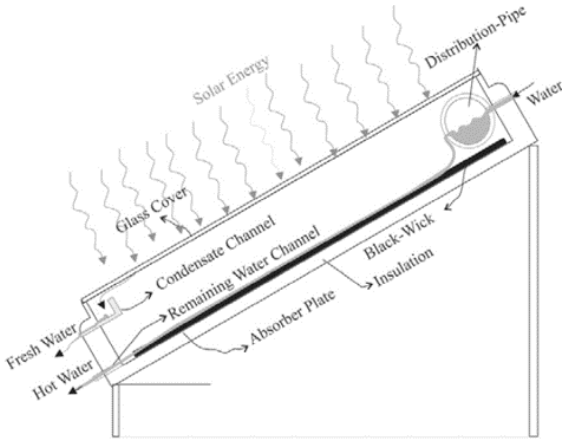

Fig. 4: Schematic diagram of inclined solar water distillation system (Aybar et al., 2005)

Validation Method

The experimental conditions were reproduced in the established OpenFOAM set-up. The mesh was a simple block generated in `blockMesh` function and subsequently rotated by using `transformPoints` utility calling -rollPitchYaw with an argument of the inclination angle. The areas of the domain occupied by solids were generated using `setFields` utility, where their dimensions were set in accordance with the experimental conditions (Appendix Tables 1 & 2).

Convection on the outer walls was simulated using `externalHeatFluxTemperature`, inputting the value of ambient temperature and of the convective heat transfer coefficient. While the ambient temperature at which experiments were performed was reported by Aybar et al. (2005), the speed of surrounding wind from which the heat transfer coefficient could be established was not measured, and hence needed to be approximated. Assuming standard weather conditions, $h = 50W/m^2K$ was used (Osczevski, 1995). The conditions for the inlet velocity were set by `flowRateInletVelocity`, specifying the values of the given flowrates. The pressure field was coupled using `fixedFluxPressure` condition for the dynamic pressure on all boundaries except the outlet, where the ambient atmospheric value was specified by `totalPressure` condition. Conversely, the velocity field was subjected to no-slip boundary condition on all walls and to `pressureInletOutletVelocity` at the outlet, so as to computationally adjust the velocity to the outlet pressure.

The optical properties of the boundaries were set as constant using `boundaryRadiationProperties` dictionary in the constant directory. The value for each boundary was set as specified by Aybar et al. (2005). The optical properties of continuous phases were set in the `radiationProperties` dictionary, where these were set as constant. It should be noted, that in future a different model for the optical properties may be employed, which would account for wavelength-dependent absorption of the transport medium and its corresponding vapours.

Finally, the remaining `radiationProperties` sub-dictionaries were set so as to match the experimental conditions. Firstly, the `solarLoad` radiation model was selected, with `sunDirTracking` sub-model for angle of incident radiation and `fairWeatherConditions` for the load. Inputs for position, time, orientation and irradiance were selected in accordance with Aybar et al. (2005). These inputs were considered to be of the highest influence on the overall results and other external influences were neglected.

Results & Discussion

The outputs of the simulations were compared in terms of water and plate temperatures and volumes of evaporated and condensed water.

Firstly, four time points were simulated and the temperature distributions on the water film were obtained (Figure 6). Water temperatures at the plate outlet were compared against the experimental values. These are presented in Figure 5. Numerically, the results follow the experimental trends, with the maximum observed offset of 5 K. This difference was attributed to the use of constant sub-models for the optical properties and the assumption regarding the external convective losses.

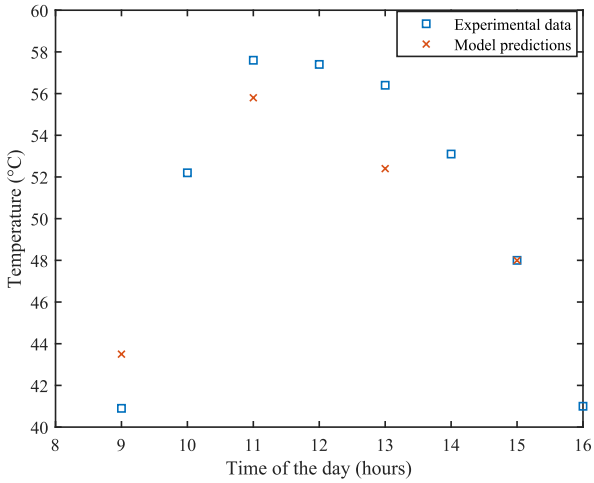

Fig. 5: Comparison of the empirical temperature points with the simulated values for the water outlet temperature

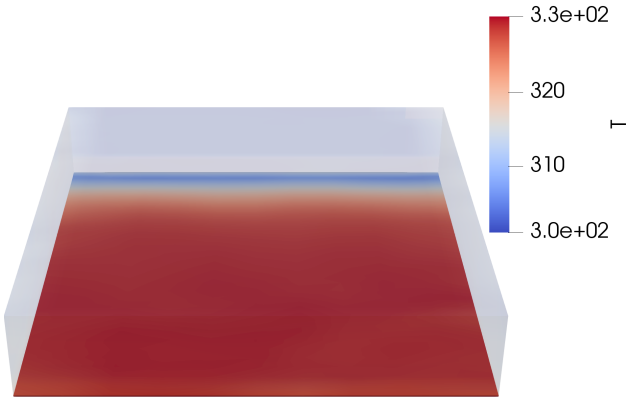

Fig. 6: Temperature distribution of the water film obtained from OpenFOAM simulations.

Time at which the temperature peak occurred was in agreement with Aybar et al. (2005), as it was observed between 11 am and noon. The time of occurrence of peak temperature corresponded to experimental observations for both plate and outlet water predictions.

As for the temperature distribution along the plate, the trend illustrated in Figures 7 and 8 was obtained. The trend is regarded intuitive, with the temperature near inlet being the lowest due to entry of cold feed, followed by somewhat plateauing temperature due to small temperature difference between the plate and the fluid. The temperature at the outlet proximity then exhibits further drop due to convective heat loss at the outlet.

Comparison of simulated peak temperatures reached by the plate against experimental values once more showed agreement within a 5 K offset. Values compared corresponded to temperatures averaged over the plate area. It should be noted that the temperature difference between the plate and fluid at the outlet increased with increasing plate temperature. Thus, it can be concluded that the minimum temperature difference between fluid and the plate that can be achieved for a given plate length increases with plate temperature.

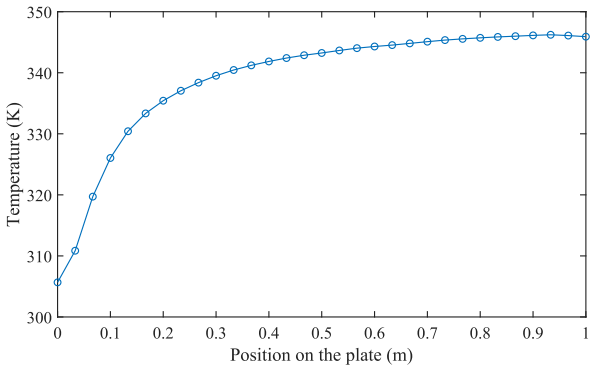

Fig. 7: 1D temperature profile on the bottom plate.

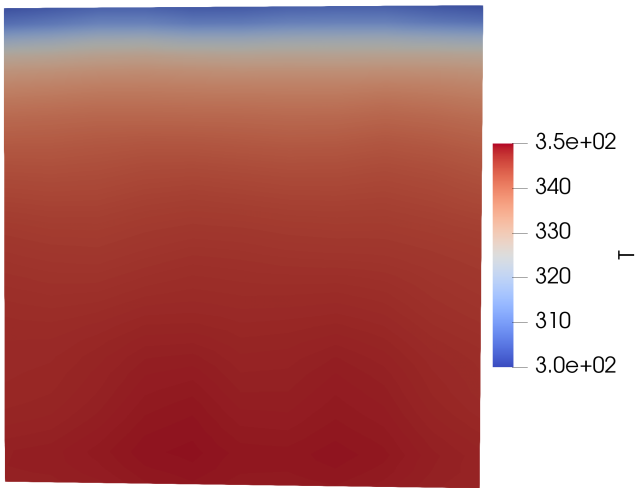

Fig. 8: 2D temperature distribution on the bottom plate obtained from OpenFOAM simulations.

Finally, level of agreement between experimentally measured and simulated values of volumes of evaporated and condensed water needed to be assessed. A conclusion on this was harder to draw, as results reported by Aybar et al. (2005) only provided cumulative values of volumes, rather than instantaneous ones. However, at any of the simulated points, the fraction of evaporated water reached a maximum value of 6 % (Figure 9). This was deemed in relative agreement with the experimentally measured average of 3-4 %. The design of the PV-T panel should account for the fact that the proportion of evaporated water rises with decreasing film thickness. This is explained by the fact that evaporation only occurs from the film surface, hence the higher the film thickness, the lower the proportion of the volume affected by this phenomenon.

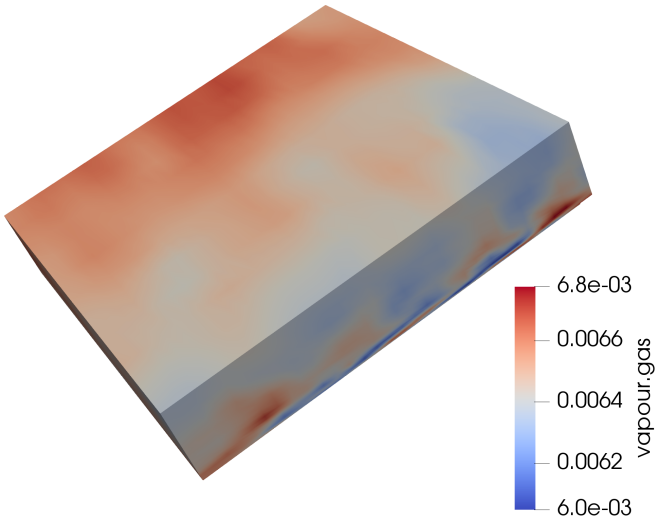

Fig. 9: Visual representation of gas-phase composition in the cavity, where red colour indicates larger water vapour fractions.

Accuracy of performance predictions

With the ultimate objective of this model being the evaluation of the PV-T collector performance, the effect of errors in the prediction of water and plate temperatures obtained from simulations on the calculation of system efficiencies is considered below.

Electrical efficiency

The linear dependence of PV electrical efficiency (η_{PV}) with cell temperature is given by the Evans-Florschuetz equation (Evans and Florschuetz, 1977):

$$\eta_{PV} = \eta_{ref}\left[1 - \beta_0\left(T_{PV} - T_{ref}\right)\right] \tag{9}$$

where β_0 is a property of the cell material and η_{ref}, specified by the manufacturer, is the PV module efficiency at reference temperature T_{ref}.

The maximum deviation in the prediction of electrical efficiency resulting from a 5 K offset between simulation results and experimental data is therefore calculated taking standard values of $\beta_0 = 0.0045K^{-1}$ and $\eta_{ref} = 0.17$ for a crystalline silicon PV module (Guarracino et al., 2016):

$$\Delta\eta_{PV}^{max} = 0.4\,\% \tag{10}$$

Thermal efficiency

Similarly, the accuracy in predictions of thermal efficiency is established. η_{th} is defined as the ratio of useful thermal output extracted (q_u) to the total solar irradiance (G):

$$\eta_{th} = \frac{q_u}{G} = \frac{\dot{m}_w C_{p_w}(T_{w,o} - T_{w,i})}{G} \tag{11}$$

For the largest error of 5 K in the prediction of water temperature at the collector outlet, the maximum deviation in thermal efficiency prediction is found to be:

$$\Delta\eta_{th}^{max} = 1\,\% \tag{12}$$

CONCLUSION & OUTLOOK

This study focused on the simulation of a free-flow PV-T water collector, presenting a method able to model this configuration, which can be used to evaluate the thermal and electrical efficiencies of the prospective design. The outlet temperature of the water film and temperature distributions on the plate predicted in this way were found to correspond to experimental values within an offset of 5 K, translating to electrical and thermal efficiency predictions within 0.4 % and 1 % accuracy respectively. Simulation results for the evaporation and condensation of the water film also showed agreement with experimental data.

The method is able to capture two-phase nature of the flow using the VOF approach, evaporation and condensation and effects of radiation. The effects of the varying geographical location, day of the year and time of the day on the irradiance are modeled. Propagation of the rays through the domain is governed by its optical properties, which are, however, in the present setup assumed constant. Therefore, an improvement can be introduced to account especially for varying absorptivity based on wavelength and thickness of the film.

To further evaluate the competitiveness of the free-flow collector compared to other designs, a parametric study of the system needs to be performed. The validated methodology presented in this work can be used to evaluate the effect of the angle of inclination of the PV module, the height of the cavity (distance between the glass cover and the PV panel), as well as the inlet temperature and flowrate of the water circulated in the system. The impact of such decisions on PV-T performance is to be established in order to adequately select design parameters that will optimise thermal and electrical efficiencies of the system as desired for the intended application.

NOMENCLATURE

α_i	fraction of a computational cell occupied by phase i
β_0	temperature coefficient (K^{-1})
Δv	specific volume change of the phase transition (m^3/kg)
$\dot{m}_w$	water mass flow rate (kg/s)
η_{PV}	PV electrical efiiciency
η_{ref}	PV standard electrical efficiency at temperature T_{ref} (K)
η_{th}	thermal efficiency
κ	thermal conductivity (W/mK)
μ	dynamic viscosity $(Pa.s)$
ϕ_{LV}	mass flux of liquid to vapour phase $(kg/s.m^2)$
ρ	fluid density (kg/m^3)
σ_{SB}	Stefan–Boltzmann constant $(5.67x10^{-8}W/m^2K^4)$
$\mathbf{F_s}$	inter-phase tension term (N/m^3)
$\mathbf{F_{sol}}$	fluid-solid interactions term (N/m^3)
$\mathbf{g}$	gravitational acceleration vector (m/s^2)
$\mathbf{U}$	velocity vector (m/s)
$\mathbf{U}_e$	interfacial velocity (m/s)
a	absorptivity
C	evaporation frequency s^{-1}
C_{pw}	specific heat capacity of water $(J/kg.K)$
E	emission contribution (W/m^3)
e	emissivity
G	irrandiance (W/m^2)
h	convective heat transfer coefficient (W/m^2K)
L	specific latent heat (J/kg)
M	molar mass (kg/mol)
p	pressure (Pa)
p_{act}	activation pressure (Pa)
p_{par}	partial pressure (Pa)
q_u	useful thermal output extracted (W/m^2)
R	gas constant $(8.314J/mol.K)$
S_h	radiative contribution to the enthalpy of the control volume (W/m^3)
T	temperature (K)
t	time (s)
T_{act}	activation temperature (K)
T_{PV}	PV operating temperature (K)
T_{ref}	reference temperature (K)
$T_{w,i}$	water temperature at collector inlet (K)
$T_{w,o}$	water temperature at collector outlet (K)

REFERENCES

[1] *2017 ASHRAE handbook.* title.

[2] Abdelrazik, A. S., Al-Sulaiman, F. A., Saidur, R., and Ben-mansour, R. (2018). "A review on recent development for the design and packaging of hybrid photovoltaic / thermal (PV/T) solar systems Design of PV". *Renewable and Sustainable Energy Reviews*, 95:110–129.

[3] Alshakhs, M.*Challenges of Solar PV in Saudi Arabia*. title.

[4] Avezov, R. R., Akhatov, J. S., and Avezova, N. R. (2011). "A Review on Photovoltaic Thermal (PV – T) Air and Water Collectors". *Applied Solar Energy*, 47(3):169–183.

[5] Aybar, H., Egeliofglu, F., and Atikol, U. (2005). "An experimental study on an inclined solar water distillation system". *Desalination*, 180:285–289.

[6] Aybar, H. (2006). "Mathematical modeling of an inclined solar water distillation system". *Desalination*, 190:63–70.

[7] BSI (2015). "BSI Standards Publication Solar heating systems for domestic hot water – Code of practice for design and installation". Technical report n°.

[8] Carey, V. P. (1992). "Liquid-vapor phase change phenomena".

[9] Charalambous, P. G., Maidment, G. G., Kalogirou, S. A., and Yiakoumetti, K. (2007). "Photovoltaic thermal (PV/T) collectors : A review". *Applied Thermal Engineering*, 27:275–286.

[10] Dubey, S., Sarvaiya, J. N., and Seshadri, B. (2013). "Temperature Dependent Photovoltaic (PV) Efficiency and Its Effect on PV Production in the World - A Review". *Energy Procedia*, 33:311–321.

[11] Evans, D. L. and Florschuetz, L. W. (1977). "Cost studies on terrestrial photovoltaic power systems with sunlight concentration". *Solar energy*, 19:255–262.

[12] Goswami, D. Y. (2015). *Principles of Solar Engineering*. Third edit ed.

[13] Guarracino, I., Mellor, A., Ekins-daukes, N. J., and Markides, C. N. (2016). "Dynamic coupled thermal-and-electrical modelling of sheet-and-tube hybrid photovoltaic / thermal (PVT) collectors". *Applied Thermal Engineering*, 101:778–795.

[14] Herrando, M., Markides, C. N., and Hellgardt, K. (2014). "A UK-based assessment of hybrid PV and solar-thermal systems for domestic heating and power : System performance". *Applied Energy*, 122:288–309.

[15] Huang, G. (2019). *Solar radiation spectrum, filtered spectrum and Si cell spectral response for a 5 mm water film, Imperial College London, UK*.

[16] Jasak, H. and Weller, H. (1998). "Interface tracking capabilities of the inter-gamma differencing scheme". , *Imperial College London, UK*.

[17] Jiwanapurkar, P. and Joshi, S. (2015). "A Review on Fluid Based Beam Splitters for Solar Photo voltaic/Thermal System". *International Journal on Recent and Innovation Trends in Computing and Communication*, 3(2).

[18] Kim, J.-H. and Kim, J.-T. (2012). "Comparison of Electrical and Thermal Performances of Glazed and Unglazed PVT Collectors". *International Journal of Photoenergy*.

[19] Lämmle, M., Oliva, A., Hermann, M., Kramer, K., and Kramer, W. (2017). "PVT collector technologies in solar thermal systems : A systematic assessment of electrical and thermal yields with the novel characteristic temperature approach". *Solar Energy*, 155:867–879.

[20] Matuska, T. (2014). "Performance and economic analysis of hybrid PVT collectors in solar DHW system". *Energy Procedia*, 48:150–156.

[21] Odeh, S. and Behnia, M. (2009). "Improving Photovoltaic Module Efficiency Using Water Cooling". *Heat Transfer Engineering*, 30(6):499–505.

[22] OECD (2011). "OECD Green Growth Studies".

[23] Osczevski, R. J. (1995). "The Basis of Wind Chill". *Arctic*, 48(4):372–382.

[24] Riffat, S. B. and Cuce, E. (2011). "A review on hybrid photovoltaic/thermal collectors and systems". *International Journal of Low-Carbon Technologies*, 6(July):212–241.

[25] Skoplaki, E. and Palyvos, J. A. (2009). "On the temperature dependence of photovoltaic module electrical performance : A review of efficiency / power correlations". *Solar Energy*, 83(5):614–624.

[26] Vivar, M. and Everett, V. (2014). "A review of optical and thermal transfer fluids used for optical adaptation or beam-splitting in concentrating solar systems". *PROGRESS IN PHOTOVOLTAICS*, 22:612–633.

[27] Voller, V. and Prakash, C. (1987). "A fixed grid numerical modelling methodology for convection-diffusion mushy phase-change problems". *Int. J. Heat Mass Transfer*, 30.

[28] Wang, K., Pantaleo, A. M., Herrando, M., Pesmazoglou, I., Franchetti, B., and Markides, C. N. (2019). "Thermoeconomic assessment of a spectral- splitting hybrid PVT system in dairy farms for combined heat and power".

[29] Zondag, H. A., Vries, D. W. D., Helden, W. G. J. V., and Zolingen, R. J. C. V. (2003). "The yield of different combined PV-thermal collector designs". 74:253–269.

APPENDIX

TABLE 1: GLASS COVER PROPERTIES OF THE INCLINED SOLAR WATER DESALINATION SYSTEM (AYBAR ET AL., 2005) (AYBAR, 2006)

Parameter	Value	Unit
Thickness	3	mm
Transmissivity	0.88	-
Emissivity	0.98	-
Inclination angle	30°	-
Distance from absorber plate	0.2	m
Length	1	m
Width	1	m
Mass	2.7	kg/m^3
Specific heat	800	J/kg.K

TABLE 2: ABSORBER PLATE PROPERTIES OF THE INCLINED SOLAR WATER DESALINATION SYSTEM (AYBAR ET AL., 2005) (AYBAR, 2006)

Parameter	Value	Unit
Material	Galvanized steel	-
Specific heat	477	J/kg.K
Absorptivity	0.96	-
Emissivity	0.08	-
Inclination angle	30°	-
Length	1	m
Width	1	m
Thickness	1	mm
Mass	7.9	kg/m^2

TABLE 3: INLET WATER PROPERTIES FOR THE INCLINED SOLAR WATER DESALINATION SYSTEM (AYBAR ET AL., 2005) (AYBAR, 2006)

Parameter	Value	Unit
Average flow rate	105.5	mL/min
Density	989	kg/m^3
Specific heat	4184	J/kg.K
Inlet Temperature	28	°C